Journal of Sound and Vibration (2002) **255**(5), 965–982
doi:10.1006/jsvi.2001.4207, available online at http://www.idealibrary.com on IDEAL®

VIBRATION ANALYSIS OF TWISTED CANTILEVERED CONICAL COMPOSITE SHELLS

J. J. Lee and C. H. Yeom

Korea Aerospace Research Institute, 52 *Oun-dong*, *Yusong-gu*, *Taejon* 305-333, *Korea*

and

I. Lee

Department of Aerospace Engineering, *Korea Advanced Institute of Science and Technology*, 373-1 *Kusong-dong*, *Yusong-gu*, *Taejon*, 305-701, *Korea*. *E-mail*: *inlee@asdl.kaist.ac.kr*

(*Received* 4 *May* 2001, *and in final form* 22 *January* 2002)

The finite element method based on the Hellinger–Reissner principle with independent strain is applied to the vibration problem of cantilevered twisted plates and cylindrical, conical laminated shells. With a small number of elements, the present assumed strain finite element method is validated by convergence tests and numerical tests, comparing with the previous published vibration results for cantilevered conical shell. Computational effort and virtual storage reduce significantly due to good convergence. This study presents the twisting angle effect on vibration characteristics of conical laminated shells. Parameter studies with varying shallowness of cylindrical and conical shells are carried out. As the curvature increases, the fundamental mode shape changes from twisting mode to bending mode. For shells with a large curvature, the fundamental frequency, which is always characterized to bending mode, is almost constant independent of twisting angle. The twisting angle affects greatly twisting frequency and mode shape.

1. INTRODUCTION

The vibration analysis of composite plates and shells has been studied for decades. The advances in composite technology have led the extensive application of composite materials in aerospace, marine and mechanical engineering. In particular, a turbo-machinery blade is preferred to be designed using composite materials due to the advantages in strength, weight, durability and design flexibility with tailoring of fiber angles in different layers.

Many researchers analyzed shell structures to obtain their vibration characteristics using semi-analytic methods and the finite element method. Among semi-analytic methods, the Rayleigh–Ritz method is extensively used. Most vibration studies using the Rayleigh–Ritz method based on Kirchhoff–Love shell theory are confined to closed cylindrical or conical shells [1–4]. The relatively few studies for vibration of open conical shells have been carried out. Srinivasan and Krishnan [5] investigated the free vibration frequencies of fully clamped opened conical shells based on Donnell's theory using an integral equation approach. Shu [6] provided the generalized differential quadrature method for the vibration analysis of conical shells. Lim and Liew [7,8] obtained natural frequencies and mode shapes for cantilevered conical shells using the Ritz method. The common drawback of most semi-analytic methods is that it is not easy to implement for various boundary conditions.

0022-460X/02/$35.00

In contrast to semi-analytic methods, independently of boundary conditions, the finite element method can be easily applied to solve vibration characteristics of shells. Many studies of thin cylindrical shells using the finite element method have been performed on vibration characteristics [9–13]. For thin structures, one main undesirable feature of shear locking is unavoidable in the finite element method. To alleviate this undesirable shear locking, the selective/reduced integration scheme [14] has been widely used in the conventional assumed displacement method. In addition, a large number of mesh elements is required to obtain good convergence. This requires a lot of virtual storage and computational effort.

As an alternative approach to overcome this shortcoming, hybrid elements, which can be constructed by introducing independent stress or strain variable, have been studied by many researchers [15]. Assumed strain elements based on Hellinger–Reissner principle have proved to be highly successful in eliminating the detrimental shear locking [16].

The present assumed strain finite element method with 40 assumed strain parameters [17] uses the degenerated solid shell element [18], which can easily handle arbitrary shell geometries and finite rotation, for the vibration analysis of twisted cylindrical and conical shells. Most propellers or turbo-machinery blades are constructed with twisting angle. The vibration analysis of cantilevered twisted laminated conical shells has not been discussed extensively except for that by commercial finite element packages in industries. The main concern of this study is to investigate the effects of twisting angle on vibration characteristics for cantilevered plates and cylindrical, conical laminated shells. The validation of the present finite element method is demonstrated by numerical tests comparing with the published results.

2. FINITE ELEMENT FORMULATION

The global position vector $\mathbf{X}$ and displacement vector $\mathbf{U}$ of a generic material point P can be expressed as follows [16]:

$$\mathbf{X} = \mathbf{X}_O + \varsigma \frac{h}{2} \mathbf{a}_3, \tag{1}$$

$$\mathbf{U} = \mathbf{U}_O + \varsigma \frac{h}{2} (\mathbf{a}'_3 - \mathbf{a}_3) \quad (-1 \leqslant \varsigma \leqslant 1), \tag{2}$$

where $\mathbf{X}_O$ and $\mathbf{U}_O$ are the position and displacement vectors of a point O on the reference plane, h is element thickness, $\mathbf{a_3}$ is the unit vector normal to the shell midsurface, $\mathbf{a}'_3$ is the $\mathbf{a}_3$ vector in the deformed configuration as shown in Figure 1.

If the rotation of $\mathbf{a}_3$ to $\mathbf{a}'_3$ is described as rotation θ_1 around $\mathbf{a}_1$ and θ_2 around $\mathbf{a}_2$, then U_ς can be expressed as

$$\mathbf{U}_\varsigma = \frac{h}{2} (\mathbf{a}'_3 - \mathbf{a}_3) = \frac{h}{2} [\theta_2 \mathbf{a}_1 + \theta_1 \mathbf{a}_2] \tag{3}$$

where $\mathbf{a}_1$ and $\mathbf{a}_2$ are orthogonal unit vectors, which are tangent to the shell midsurface. For a degenerated solid shell element, the position vector and the displacement vector of point **P** are interpolated in the finite element using their corresponding nodal values. Introducing

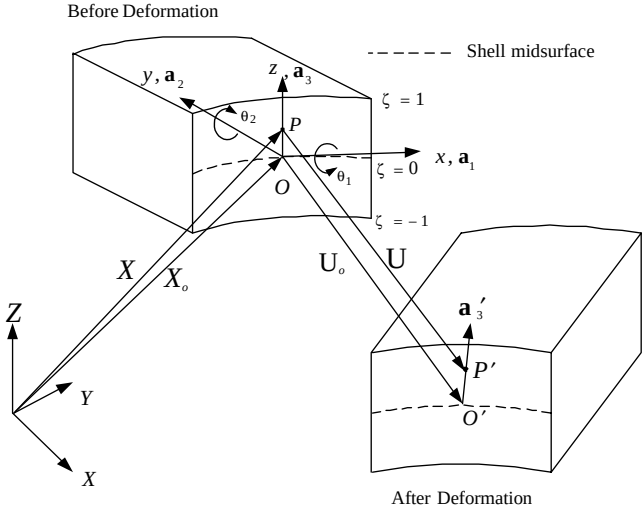

Figure 1. Kinematics of shell deformation.

the shape function $\mathbf{N}$ of nine-node element, equations (1) and (2) can be rewritten as

$$\mathbf{X} = \sum_j \mathbf{N}_j[\mathbf{X}_O]_j + \varsigma \sum_j \mathbf{N}_j \left[\frac{h}{2}\mathbf{a}_3\right]_j, \qquad \mathbf{U} = \sum_j \mathbf{N}_j[\mathbf{U}_O]_j + \varsigma \sum_j \mathbf{N}_j[\mathbf{U}_\varsigma]_j \tag{4, 5}$$

where subscript j means node number j in the element.

For a solid in equilibrium by introducing the principle of virtual work, the formulation is expressed as

$$\int_V (\delta\bar{\boldsymbol{\varepsilon}})^{\mathrm{T}}\boldsymbol{\sigma}\,\mathrm{d}V + \int_V \delta\mathbf{U}\rho\ddot{\mathbf{U}}\,\mathrm{d}V = 0, \tag{6}$$

where $\delta\bar{\boldsymbol{\varepsilon}}$ is the virtual strain vector, $\boldsymbol{\sigma}$ is the stress vector, $\delta\mathbf{U}$ is the virtual displacement vector, ρ is the mass density and V is the volume.

Introducing an independent strain vector $\boldsymbol{\varepsilon}$ and the displacement-dependent strain vector $\bar{\boldsymbol{\varepsilon}}$, the compatibility condition is expressed as

$$\int_V (\delta\boldsymbol{\sigma})^{\mathrm{T}}(\bar{\boldsymbol{\varepsilon}} - \boldsymbol{\varepsilon})\,\mathrm{d}V = 0, \tag{7}$$

where $\delta\boldsymbol{\sigma}$ is the virtual stress vector.

The stress vector $\boldsymbol{\sigma}$ is related to material elastic constant matrix $\mathbf{C}$ and independent strain vector $\boldsymbol{\varepsilon}$. Then

$$\boldsymbol{\sigma} = \mathbf{C}\boldsymbol{\varepsilon} \tag{8}$$

For the analysis of composite shells, the displacement-dependent strain $\bar{\boldsymbol{\varepsilon}}$ and the displacement-independent strain $\boldsymbol{\varepsilon}$ are assumed to vary linearly through the shell thickness. The assumption is expressed as follows:

$$\bar{\boldsymbol{\varepsilon}} = \bar{\boldsymbol{\varepsilon}}_O + \varsigma\bar{\boldsymbol{\varepsilon}}_\varsigma, \qquad \boldsymbol{\varepsilon} = \boldsymbol{\varepsilon}_O + \varsigma\boldsymbol{\varepsilon}_\varsigma, \tag{9}$$

In equation (9), $\bar{\boldsymbol{\varepsilon}}_O$, $\bar{\boldsymbol{\varepsilon}}_\varsigma$, and $\boldsymbol{\varepsilon}_O$, $\boldsymbol{\varepsilon}_\varsigma$, are independent of ς. Also, they are defined in the form as follows:

$$\bar{\boldsymbol{\varepsilon}}_O = \tfrac{1}{2}(\bar{\boldsymbol{\varepsilon}}_\beta + \bar{\boldsymbol{\varepsilon}}_{-\beta}), \qquad \bar{\boldsymbol{\varepsilon}}_\varsigma = \frac{1}{2\beta}(\bar{\boldsymbol{\varepsilon}}_\beta - \bar{\boldsymbol{\varepsilon}}_{-\beta}),$$

$$\boldsymbol{\varepsilon}_O = \tfrac{1}{2}(\boldsymbol{\varepsilon}_\beta + \boldsymbol{\varepsilon}_{-\beta}), \qquad \boldsymbol{\varepsilon}_\varsigma = \frac{1}{2\beta}(\boldsymbol{\varepsilon}_\beta - \boldsymbol{\varepsilon}_{-\beta}), \tag{10}$$

where subscripts β and $-\beta$ denote its values at $\varsigma = \beta$ and $\varsigma = -\beta$. In this study, β is chosen as $\beta = 1/\sqrt{3}$ in accordance with the two-point Gaussian integration rule. By the relations between the global Cartesian co-ordinate system (X, Y, Z) and the normalized nodal co-ordinate system (ξ, η, ς), matrix $\mathbf{J}$ is defined as

$$\mathbf{J} = \begin{bmatrix} \dfrac{\partial X}{\partial \xi} & \dfrac{\partial \mathrm{Y}}{\partial \xi} & \dfrac{\partial \mathrm{Z}}{\partial \xi} \\ \dfrac{\partial \mathrm{X}}{\partial \eta} & \dfrac{\partial \mathrm{Y}}{\partial \eta} & \dfrac{\partial \mathrm{Z}}{\partial \eta} \\ \dfrac{\partial \mathrm{X}}{\partial \zeta} & \dfrac{\partial \mathrm{Y}}{\partial \zeta} & \dfrac{\partial \mathrm{Z}}{\partial \zeta} \end{bmatrix}. \tag{11}$$

Using equation (4), the Jacobian matrix of an element can be expressed as

$$\mathbf{J} = \begin{bmatrix} \sum \mathbf{N}_{j,\xi}(\mathbf{X}_O)_j & \sum \mathbf{N}_{j,\xi}(\mathbf{Y}_O)_j & \sum \mathbf{N}_{j,\xi}(\mathbf{Z}_O)_j \\ \sum \mathbf{N}_{j,\eta}(\mathbf{X}_O)_j & \sum \mathbf{N}_{j,\eta}(\mathbf{Y}_O)_j & \sum \mathbf{N}_{j,\eta}(\mathbf{Z}_O)_j \\ \sum \mathbf{N}_j\left(\dfrac{h}{2}a_{31}\right)_j & \sum \mathbf{N}_j\left(\dfrac{h}{2}a_{32}\right)_j & \sum \mathbf{N}_j\left(\dfrac{h}{2}a_{33}\right)_j \end{bmatrix}$$

$$+ \varsigma \begin{bmatrix} \sum \mathbf{N}_{j,\xi}\left(\dfrac{h}{2}a_{31}\right)_j & \sum \mathbf{N}_{j,\xi}\left(\dfrac{h}{2}a_{32}\right)_j & \sum \mathbf{N}_{j,\xi}\left(\dfrac{h}{2}a_{33}\right)_j \\ \sum \mathbf{N}_{j,\eta}\left(\dfrac{h}{2}a_{31}\right)_j & \sum \mathbf{N}_{j,\eta}\left(\dfrac{h}{2}a_{32}\right)_j & \sum \mathbf{N}_{j,\eta}\left(\dfrac{h}{2}a_{33}\right)_j \\ 0 & 0 & 0 \end{bmatrix}$$

$$= \mathbf{J}_O + \varsigma \mathbf{J}_\varsigma. \tag{12}$$

The determinant J of Jacobian matrix is also assumed to vary linearly in the thickness direction. Then

$$J(\xi, \eta, \varsigma) = J_O(\xi, \eta) + \varsigma J_\varsigma(\xi, \eta)$$

$$= (1 + r\varsigma) J_O \tag{13}$$

where J_O, J_ς and r are defined as

$$J_O(\xi, \eta) = \tfrac{1}{2}(J_\beta + J_{-\beta}), \qquad J_\varsigma(\xi, \eta) = \frac{1}{2\beta}(J_\beta - J_{-\beta}),$$

$$r(\xi, \eta) = \frac{J_\varsigma(\xi, \eta)}{J_O(\xi, \eta)}. \tag{14}$$

The linear assumption of strain and the determinant of the Jacobian matrix through the thickness allows analytical integration in the thickness direction for laminated composite shells.

Introducing isoparametric shape functions $\mathbf{N}$ of nine-node element, nodal degrees of freedom $\mathbf{q}_e$ with five components $(u, v, w, \theta_1, \theta_2)$,

$$\mathbf{U} = \mathbf{N}\mathbf{q}_e, \qquad \bar{\boldsymbol{\varepsilon}} = \mathbf{B}\mathbf{q}_e, \tag{15, 16}$$

where $\mathbf{B}$ is a matrix relating strain to displacement.

Choosing a set of 40 assumed strain parameters $\boldsymbol{\alpha}$, the assumed displacement-independent strain is

$$\boldsymbol{\varepsilon} = \mathbf{P}\boldsymbol{\alpha} \tag{17}$$

in which the size of $\mathbf{P}$ matrix is 5×40. For details on assumed strain parameters, see reference [17].

Utilizing equations (8), (15), (16) and (17), the compatibility condition, i.e., equation (7), and the strain energy term in equation (6) can be written as follows:

$$\sum \delta\alpha^{\mathrm{T}}(\mathbf{G}\mathbf{q}_e - \mathbf{H}\boldsymbol{\varepsilon}) = 0, \qquad \int \delta\bar{\boldsymbol{\varepsilon}}^{\mathrm{T}}\boldsymbol{\sigma}\,\mathrm{d}V_e = \sum \delta\mathbf{q}_e^{\mathbf{T}}(\mathbf{G}^{\mathrm{T}}\boldsymbol{\alpha})\,\mathrm{d}A_e \tag{18, 19}$$

with

$$\mathbf{G} = \int \mathbf{P}^{\mathrm{T}}\mathbf{C}\mathbf{B}\,\mathrm{d}A_e, \quad \mathbf{H} = \int \mathbf{P}^{\mathrm{T}}\mathbf{C}\mathbf{P}\,\mathrm{d}A_e, \quad \mathrm{d}A_e = J_O\,\mathrm{d}\xi\,\mathrm{d}\eta, \tag{20a–c}$$

where the summation sign indicates assembly over all elements.

From equation (18), $\boldsymbol{\alpha}$ can be obtained. Then

$$\boldsymbol{\alpha} = \mathbf{H}^{-1}\mathbf{G}\mathbf{q}_e. \tag{21}$$

Assuming simple harmonic motion for small amplitude vibration, the displacement vector can be expressed as

$$\begin{aligned}\mathbf{U} &= \mathrm{e}^{\mathrm{i}\omega t}\mathbf{U} \\ &= \mathrm{e}^{\mathrm{i}\omega t}\mathbf{N}^*\mathbf{q}_e,\end{aligned} \tag{22}$$

where

$$\begin{aligned}\mathbf{N}^* &= \sum_j \mathbf{N}_j[\mathbf{U}_O]_j + \varsigma \sum_j \mathbf{N}_j[\mathbf{U}_\varsigma]_j \\ &= \mathbf{N}_O^* + \varsigma\mathbf{N}_\varsigma^*\end{aligned} \tag{23}$$

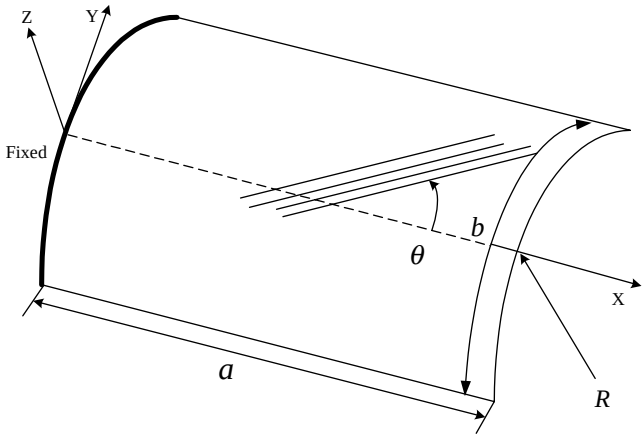

Figure 2. Configuration of cylindrical shell.

Using equations (5) and (22), the kinetic energy term becomes

$$\int \delta \mathbf{U}^{\mathrm{T}} \rho \ddot{\mathbf{U}} \, \mathrm{d}V = -\omega^2 \sum \delta \mathbf{q}_e^{\mathrm{T}} (\mathbf{N}^{*\mathrm{T}} \rho \mathbf{N}^*) \, \mathrm{d}A_e. \tag{24}$$

Introducing equations (19), (21) and (24), the equilibrium equation (equation (6)) is transformed into an eigenvalue problem as follows:

$$\mathbf{Kq} = \omega^2 \mathbf{Mq} \tag{25}$$

with

$$\mathbf{K} = \mathbf{G}^{\mathrm{T}} \mathbf{H}^{-1} \mathbf{G}, \qquad \mathbf{M} = \rho \mathbf{N}^{*\mathrm{T}} \mathbf{N}^* \tag{26}$$

where **K** and **M** are the global stiffness and mass matrices respectively.

3. VERIFICATION AND COMPARISON

The present finite element method is based on degenerated solid element with five degrees of freedom. The present method is applicable for plates and shells with arbitrary shapes (cylindrical, spherical and conical shells) except for very thick structures. Applying two point integration of Gaussian rule through the thickness direction, strains can be computed more accurately than the first order shear deformable theory. For the validity and reliability of the present vibration analysis code, the vibration characteristics of cantilevered plates and cylindrical, conical shells are compared with those of published papers.

Shell configurations are shown in Figure 2. First, the vibration frequencies of a cantilevered plate and shell are investigated using a mesh division with 4×6 elements. The graphite/epoxy material properties are described in Table 1.

For graphite/epoxy cantilevered laminated $[\pm 45/\mp 45]_s$ plate with $a/b = 2$, $h = 1{\cdot}04$ mm and $b = 76{\cdot}2$ mm, The first five frequencies are illustrated in Table 2. The present results are in good agreement with the calculated and experimental results of Crawley [10] and finite element results of Ottia *et al.* [13].

For graphite/epoxy cantilevered laminates of $[0/0/\pm 30]_s$ cylindrical panel, as shown in Figure 2, with $a/b = 2$, $h = 1{\cdot}04$ mm, $b = 76{\cdot}2$ mm and $R = 127$ mm, the results are illustrated in Table 3. The present finite element results obtained by the small number of elements have lower natural frequencies than the previous finite element results and are very close to the experimental results [10, 13].

TABLE 1

Material properties

	Graphite/epoxy	E-glass/epoxy
E_1	128 Gpa	60·7 GPa
E_2	11 Gpa	24·8 GPa
G_{12}	4·48 Gpa	12·0 GPa
G_{23}	4·48 Gpa	12·0 GPa
G_{13}	4·48 Gpa	12·0 GPa
v_{12}	0·25	0·23
ρ	1500 kg/m^3	2000 kg/m^3

TABLE 2

Comparison of vibration frequencies (Hz) *of cantilevered* $[45/-45/-45/45]_s$ *graphite/epoxy plate with* $a/b = 2$, $h = 1{\cdot}04\,mm$ *and* $b = 76{\cdot}2\,mm$[†]

Mode	Present	Reference [10]	Reference [13]
1	31·54	31·9 (31·3[†])	31·85
2	189·3	191·3 (185·8[†])	191·16
3	224·3	228·2 (214·0[†])	228·2
4	557·5	565·2 (533·0[†])	562·2
5	694·3	708·3 (653·0[†])	653·0

[†]The values in parentheses are experimental results.

Next, natural frequencies of a cantilevered conical shallow shell with the lamination of $[-\theta/\theta]_s$ are investigated. Consider thin shallow conical shell with length a, base cone arc length b_O, thickness h, vertex angle θ_v and subtended angle ϕ. The E-glass/epoxy conical shell geometry, as shown in Figure 3, has $a/h = 100$, $a/b_O = 1{\cdot}5$, $\theta_v = 15^\circ$ and $\phi = 30^\circ$. The material uses E-glass/epoxy of Table 1.

Comparison of Ritz method and finite element package solutions is shown in Figure 4. The non-dimensional frequency parameters $\lambda^* = \omega a\sqrt{v_{12}/E_1}$ of cantilevered conical shells, with various fiber orientation θ, are very close to the results of Lim *et al.* [8] obtained using Ritz method and the results of LUSAS (a finite element package), obtained by 15×30 elements [8]. Even with the small number of elements, the present solutions have a good agreement with Ritz method and finite element package solutions.

4. NUMERICAL RESULTS AND DISCUSSIONS

4.1. TWISTED CANTILEVERED PLATES AND CYLINDRICAL SHELLS

Consider a twisted cantilevered plate and shell where the twisting angle φ ranges from 0 to 90°. The lamination consists of graphite/epoxy $[0/\pm 45/90]_s$ for plates and shells. The

TABLE 3

Comparison of vibration frequencies (Hz) *of cantilevered* $[0/0/\pm 30]_s$ *graphite/epoxy cylindrical shell with* $a/b = 2$, $R = 127\,mm$, $h = 1{\cdot}04\,mm$ *and* $b = 76{\cdot}2\,mm$

Mode	Present	Reference [10]	Reference [13]
1	165·5	165·7 (161·0†)	168·7
2	285·5	289·6 (245·1†)	295·1
3	598·3	597·1 (555·6†)	606·1
4	710·5	718·5 (670·0†)	713·0
5	825·0	833·3 (794·0†)	816·94

†The values in parentheses are experimental results.

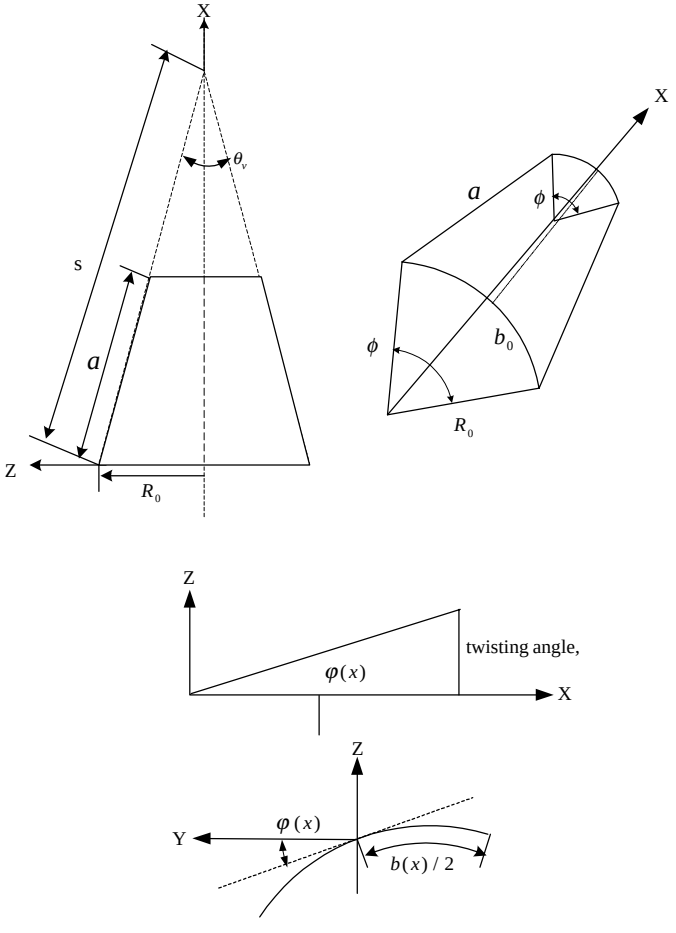

Figure 3. Configuration of twisted conical shell.

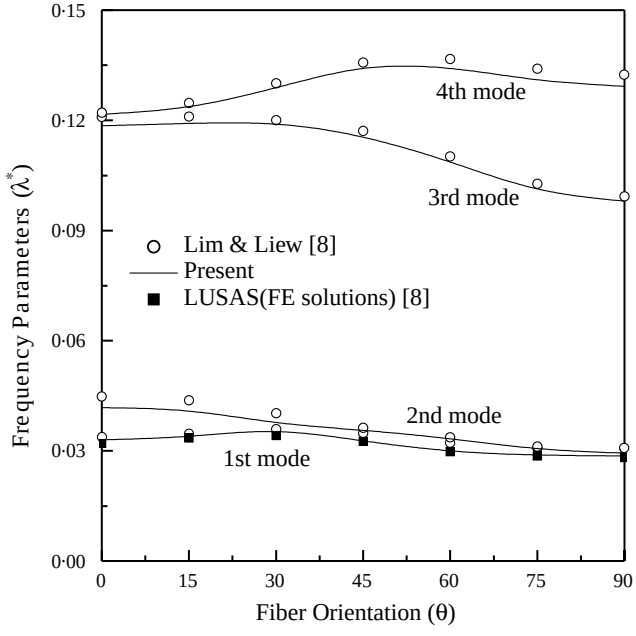

Figure 4. Comparison of frequency parameter ($\lambda^* = \omega a\sqrt{v_{12}/E_1}$) for cantilevered conical $[-\theta/\theta]_s$ E-glass/epoxy shells with $a/h = 100$, $\theta_v = 15^\circ$ $a/b_O = 1{\cdot}5$ and $\phi = 30^\circ$.

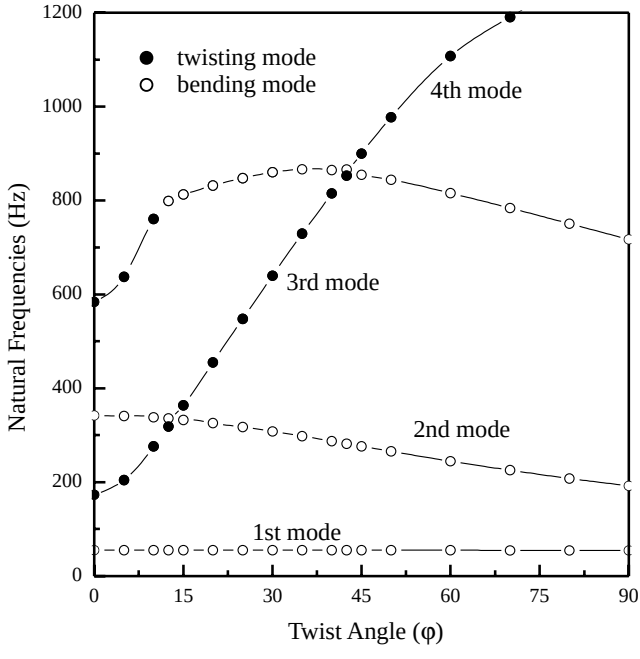

Figure 5. Effects of twisting angle φ on natural frequencies $\lambda = \omega a\sqrt{v_{12}/E_2}$ for cantilevered $[0/\pm 45/90]_s$ graphite/epoxy plates with $a/b = 2$, $b = 76{\cdot}2$ mm and $h = 1{\cdot}04$ mm.

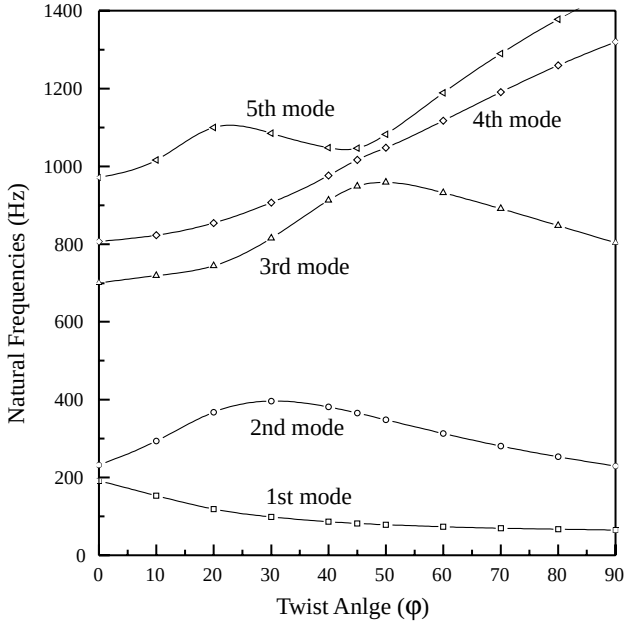

Figure 6. Effects of twisting angle φ on natural frequencies $\lambda = \omega a\sqrt{v_{12}/E_2}$ for cantilevered $[0/\pm 45/90]_s$ graphite/epoxy shells with $a/b = 2$, $b = 76{\cdot}2$ mm, $h = 1{\cdot}04$ mm and $R = 127$ mm.

TABLE 4

Effects of shallowness ratio for twisted cantilevered cylindrical $[0/\pm 45/90]_s$ *graphite/epoxy shells with* $a/b = 2$, $b = 76{\cdot}2\,mm$, $h = 1{\cdot}04\,mm$ *and* $\varphi = 20^\circ$

	Mode				
R/b	1	2	3	4	5
1	171·65	435·25	827·06	902·00	1285·50
2	105·01	356·76	700·14	856·65	1020·90
3	82·83	344·49	601·97	854·02	937·33
4	72·90	340·50	547·21	843·73	933·40
5	67·57	338·24	516·74	837·28	940·75
10	59·12	332·50	471·01	829·85	965·99
100	55·36	326·47	455·63	830·93	966·97
Plate	55·22	325·90	455·21	831·82	963·51

twisting angle is defined as shown in Figure 3. The twisting angle is assumed to vary linearly in the x-direction with reference to the center of the half-width ($b/2$).

Figure 5 shows the effect of twisting angles on natural frequencies of cantilevered $[0/\pm 45/90]_s$ plates. The fundamental frequency, which is always characterized to the first bending mode, is almost constant independently of twisting angle φ. As the twisting angle increases up to $\varphi = 15^\circ$, the second frequency of the first twisting mode increases. Beyond $\varphi = 15^\circ$, the second vibration mode changes from the first twisting mode to the second bending mode. The twisting angle affects greatly twisting and higher bending modes for cantilevered plates. The twisting angle improves significantly vibration frequencies of twisting modes.

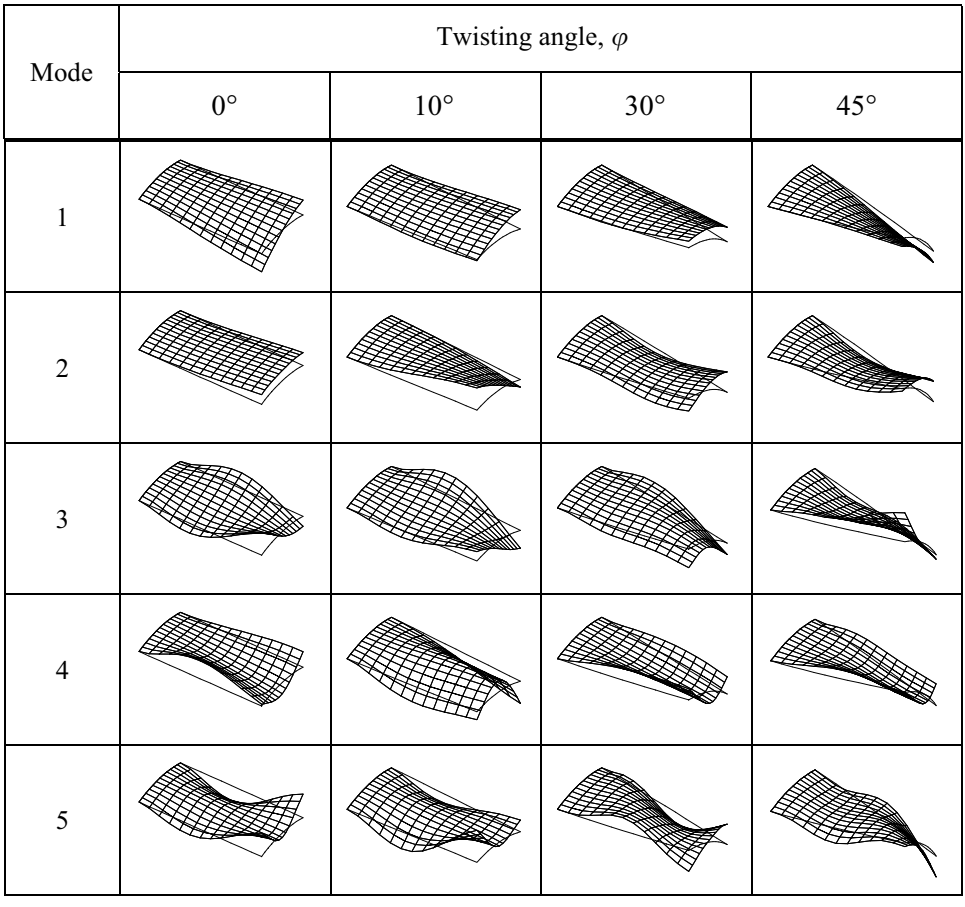

Figure 7. Mode shapes of various twisted cantilevered $[0/\pm 45/90]_s$ graphite/epoxy shells with $a/b = 2$, $b = 76{\cdot}2$ mm, $h = 1{\cdot}04$ mm and $R = 127$ mm.

TABLE 5

Convergence test for non-dimensional frequencies ($\lambda = \omega a\sqrt{\rho/E_2}$) *for twisted cantilevered conical graphite/epoxy* $[\pm 45]_s$ *shells with* $a/h = 100$, $s/a = 5$, $\theta_v = 15^\circ$, $\phi = 30^\circ$ *and* $\varphi = 15^\circ$

	Mode frequencies				
Element division	1	2	3	4	5
4×4	0·03332	0·16794	0·19023	0·44162	0·48242
5×5	0·03329	0·16764	0·18939	0·44006	0·47891
6×6	0·03327	0·16750	0·18905	0·43925	0·47747
7×7	0·03326	0·16741	0·18888	0·43877	0·47673
8×8	0·03325	0·16735	0·18879	0·43844	0·47629
9×9	0·03324	0·16731	0·18873	0·43818	0·47603
10×10	0·03323	0·16727	0·18868	0·43800	0·47585

Figure 6 shows the results on the effects of twisting angles on natural frequencies for cantilevered $[0/\pm 45/90]_s$ cylindrical shell with $R = 127$ mm. Vibration mode shapes corresponding to natural frequencies are shown in Figure 7. The boundary line indicates the

Mode	R/b			
	1	2	5	plate
1	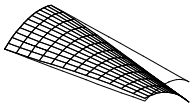	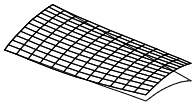	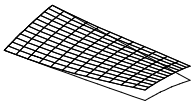	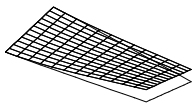
2	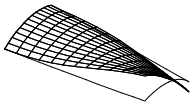	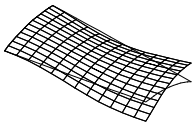	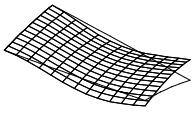	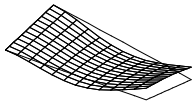
3	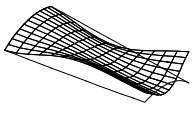	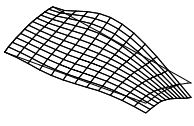	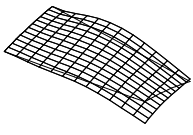	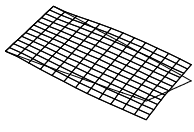
4	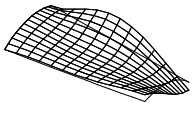	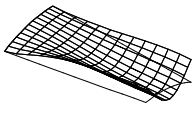	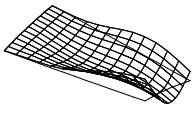	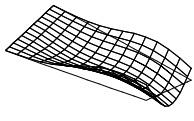
5	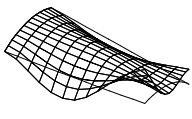	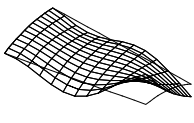	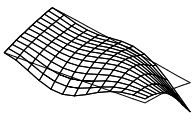	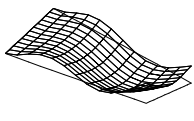

Figure 8. Mode shapes of twisted cantilevered $[0/\pm 45/90]_s$ graphite/epoxy shells with $a/b = 2$, $b = 76{\cdot}2\,\text{mm}$, $h = 1{\cdot}04\,\text{mm}$ and $R = 127\,\text{mm}$ for various shallow ratio.

original undeformed shape. As the twisting angle increases, the first frequency decreases and the corresponding mode shape also changes. It is observed that bending modes become lower modes with increase in twisting angle. For $\varphi = 20^\circ$, the natural frequencies of the first five modes are distributed in wide ranges. It is desirable to have a separation of the lower vibration modes for design considerations.

Table 4 presents the effect of shallowness ratio on vibration frequencies for twisted cylindrical shells with a twisting angle $\varphi = 20^\circ$. Figure 8 shows mode shapes corresponding to the natural frequencies. As shallowness (R/b_O) increases, all frequencies reduce and the first mode becomes bending mode. This is because the curvature influences stiffness and hence natural frequencies.

4.2. TWISTED CANTILEVERED CONICAL SHELLS

Consider a twisted conical shell with $a/h = 100$, $s/a = 5$, $\theta_v = 15^\circ$, $\phi = 30^\circ$ and $\varphi = 15^\circ$. To confirm the convergence of solution, convergence test is conducted. The convergence of non-dimensional frequencies $(\lambda = \omega a\sqrt{\rho/E_2})$ for its conical shell with graphite/epoxy $[\pm 45]_s$ lamination is presented in Table 5. The number of elements increases from 4×4

TABLE 6

Non-dimensional frequencies ($\lambda = \omega a\sqrt{\rho/E_2}$) *for twisted cantilevered conical* $[\pm 45]_s$ *graphite/epoxy shells with* $a/h = 100$, $s/a = 5$ *and* $\theta_v = 15^\circ$

Subtended angle, ϕ	Twisting angle, φ	Mode				
		1	2	3	4	5
60	0	0·10334	0·11866	0·31734	0·38582	0·47452
	15	0·08640	0·14414	0·32905	0·41381	0·47821
	30	0·06585	0·17619	0·34067	0·41447	0·51462
	45	0·05230	0·18061	0·36731	0·41942	0·50679
	60	0·04336	0·15995	0·41019	0·41883	0·48279
	75	0·03728	0·13354	0·38519	0·45007	0·49970
	90	0·03302	0·11041	0·34275	0·47684	0·53512
45	0	0·06798	0·12225	0·35665	0·35985	0·62518
	15	0·06210	0·13846	0·31263	0·41817	0·61466
	30	0·05089	0·16285	0·28067	0·44693	0·62330
	45	0·04241	0·16102	0·28810	0·43707	0·63811
	60	0·03655	0·13877	0·32444	0·40768	0·64671
	75	0·03247	0·11577	0·34997	0·38962	0·65181
	90	0·02957	0·09688	0·32279	0·42356	0·64992
30	0	0·0331	0·1658	0·1884	0·4312	0·4706
	15	0·0333	0·1675	0·1891	0·4393	0·4775
	30	0·0318	0·1546	0·2007	0·4273	0·4980
	45	0·0297	0·1327	0·2256	0·3920	0·5394
	60	0·0276	0·1118	0·2561	0·3543	0·5814
	75	0·0259	0·0944	0·2885	0·3198	0·6056
	90	0·0244	0·0805	0·2858	0·3252	0·5949
15	0	0·0156	0·0924	0·2165	0·2586	0·3025
	15	0·0158	0·0903	0·2208	0·2616	0·3034
	30	0·0159	0·0839	0·2285	0·2690	0·3064
	45	0·0160	0·0759	0·2291	0·2878	0·3114
	60	0·0161	0·0681	0·2225	0·3130	0·3200
	75	0·0162	0·0610	0·2127	0·3242	0·3456
	90	0·0163	0·0549	0·2017	0·3332	0·3693

meshes to 10×10 meshes. As observed, the present solutions have excellent convergence. Comparing with 4×4 and 10×10 meshes, the results by 4×4 mesh have a deviation of less 1% from those of 10×10 mesh for the first four frequencies.

For four types of subtended angles with $\phi = 15^\circ$, $\phi = 30^\circ$, $\phi = 45^\circ$ and $\phi = 60^\circ$, the results of the effects of twisting angles φ on the non-dimensional frequencies of graphite/epoxy cantilevered $[\pm 45]_s$ conical shells with $a/h = 100$, $s/a = 5$ and $\theta_v = 15^\circ$ is presented in Table 6. For conical shell with $\phi = 15^\circ$, as the twisting angle φ increases, there is no significant change in fundamental frequencies for various twisting angles and the second frequencies decrease. For conical shells with $\phi \geqslant 30^\circ$, as the twisting angle φ increases, the first frequencies decrease. An increase in the subtended angle indicates an increase in the depth of a shell. For a deeper shell, the twisting angle affects greatly the fundamental frequencies.

Figures 9 and 10 show the mode shapes for the cantilevered twisted $[\pm 45]_s$ conical shell with a subtended angle $\phi = 60^\circ$ and $\phi = 45^\circ$ respectively. Note that there is a change in the first vibrating modes: one is twisting mode and the other is bending mode.

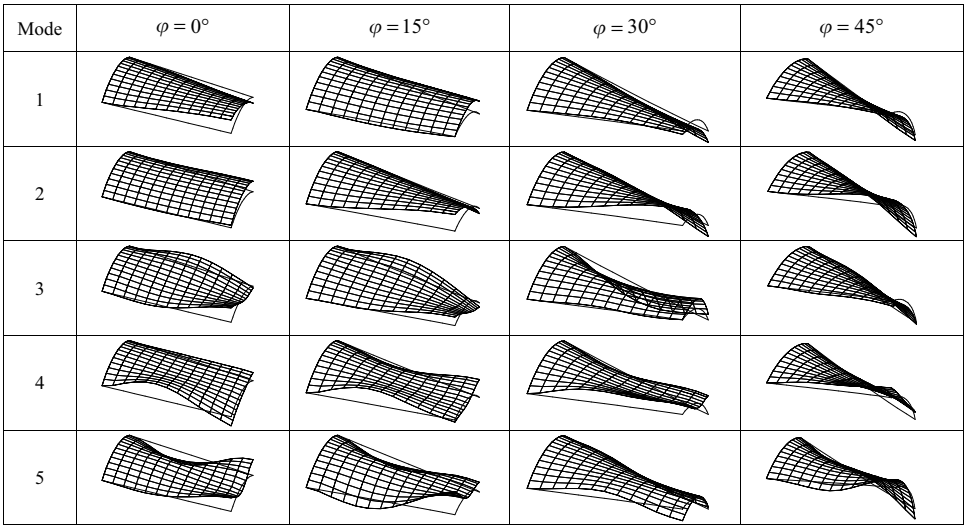

Figure 9. Mode shapes of twisted cantilevered $[\pm 45]_s$ graphite/epoxy shells with $a/h = 100$, $s/a = 5$, $\theta_v = 15^\circ$ and $\phi = 60^\circ$.

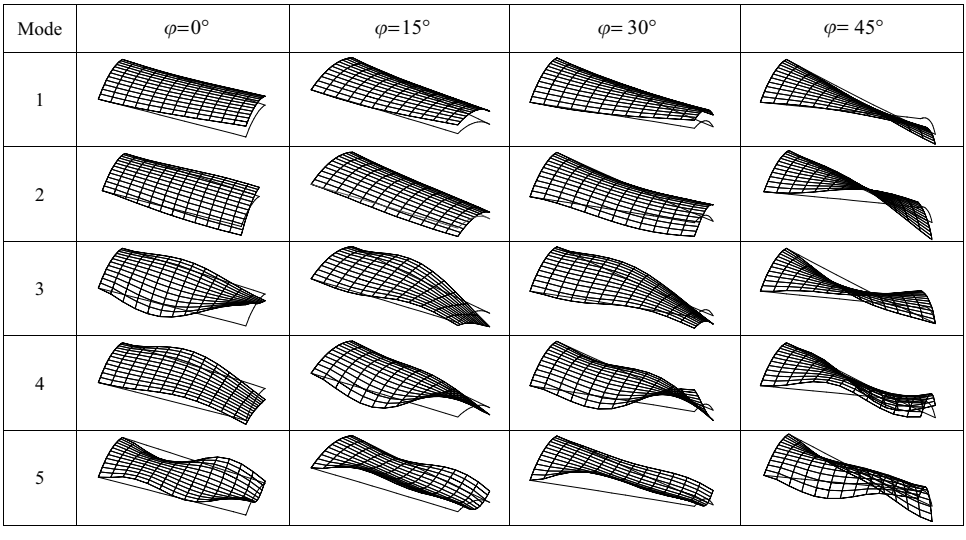

Figure 10. Mode shapes of twisted cantilevered $[\pm 45]_s$ graphite/epoxy shells with $a/h = 100$, $s/a = 5$, $\theta_v = 15^\circ$ and $\phi = 45^\circ$.

Here, the effects of the fiber orientation on the vibration characteristics is investigated for a pretwisted cantilevered $[\pm\theta]_s$ conical shell with $a/h = 100$, $s/a = 5$, $\theta_v = 15^\circ$ and $\varphi = 30^\circ$. Figure 11 shows the results of the non-dimensional frequencies $\lambda = \omega a\sqrt{v_{12}/E_2}$ for pretwisted moderately deep shell with $\phi = 30^\circ$. Up to fiber orientations $\theta = 20^\circ$, the first five frequencies increase. For $\theta > 20^\circ$, the fiber orientation significantly affects higher frequencies. Figure 12 shows the non-dimensional frequencies $\lambda = \omega a\sqrt{v_{12}/E_2}$ for pretwisted shallow shell with $\phi = 10^\circ$. All frequencies decrease except for the third frequency for all fiber orientation.

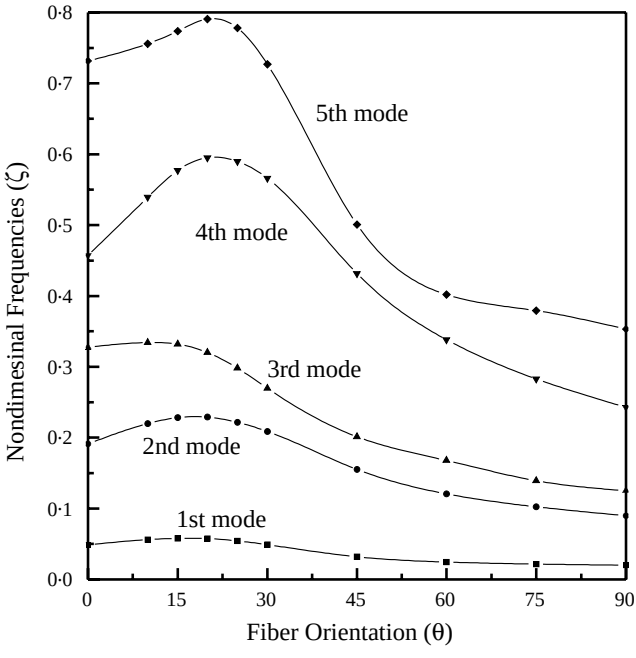

Figure 11. Effects of fiber orientation on the non-dimensional frequencies $\lambda = \omega a\sqrt{v_{12}/E_2}$ for twisted cantilevered $[\pm\theta]_s$ graphite/epoxy shells with $a/h = 100$, $s/a = 5$, $\theta_v = 15^\circ$, $\varphi = 30^\circ$ and $\phi = 30^\circ$.

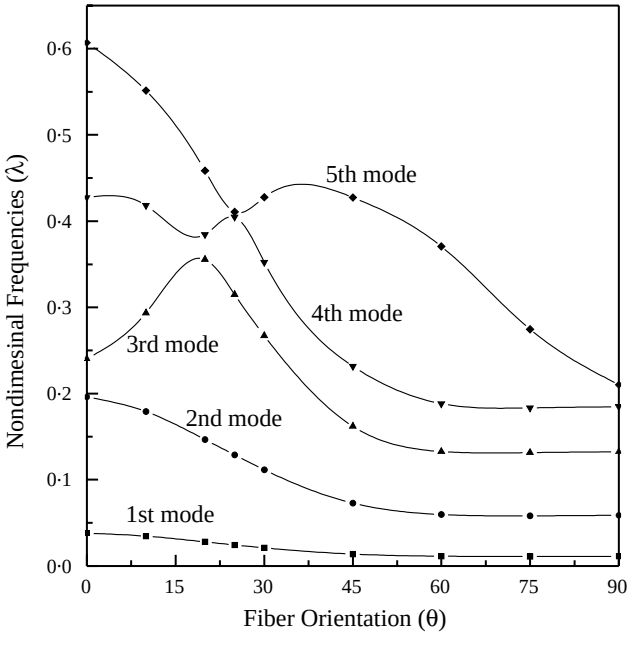

Figure 12. Effects of fiber orientation on the non-dimensional frequencies $\lambda = \omega a\sqrt{v_{12}/E_2}$ for twisted cantilevered $[\pm\theta]_s$ graphite/epoxy shells with $a/h = 100$, $s/a = 5$, $\theta_v = 15^\circ$, $\varphi = 30^\circ$ and $\phi = 10^\circ$.

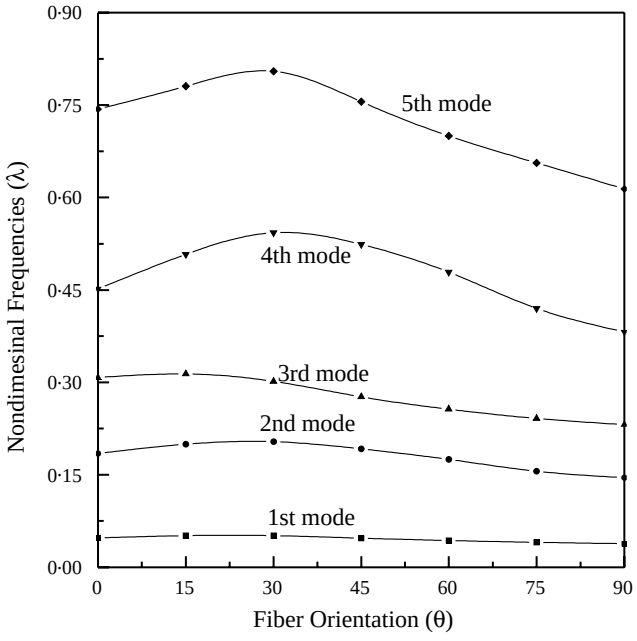

Figure 13. Effects of fiber orientation on the non-dimensional frequencies $\lambda = \omega a\sqrt{v_{12}/E_2}$ for twisted cantilevered $[0/\pm\theta/90]_s$ graphite/epoxy shells with $a/h = 100$, $s/a = 5$, $\theta_v = 15^\circ$, $\varphi = 30^\circ$ and $\phi = 30^\circ$.

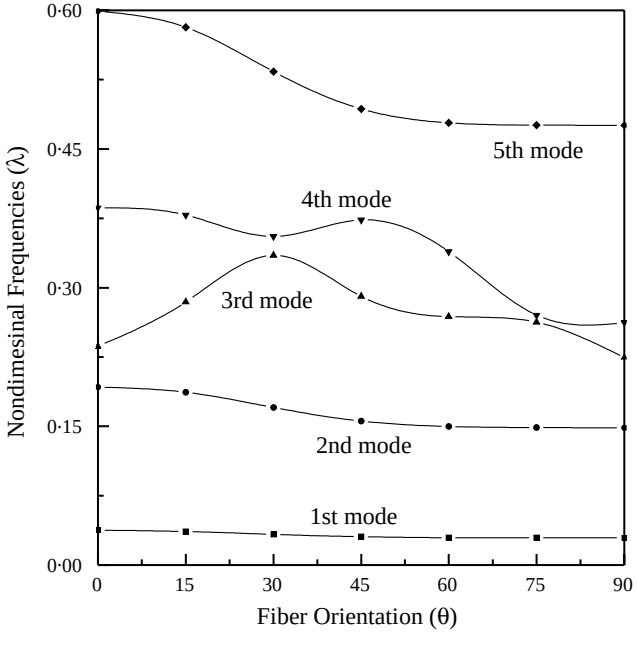

Figure 14. Effects of fiber orientation on the non-dimensional frequencies $\lambda = \omega a\sqrt{v_{12}/E_2}$ for twisted cantilevered $[0/\pm\theta/90]_s$ graphite/epoxy shells with $a/h = 100$, $s/a = 5$, $\theta_v = 15^\circ$, $\varphi = 30^\circ$ and $\phi = 10^\circ$.

Consider a conical shell with $[0/\pm\theta/90]_s$ where the material is graphite/epoxy and the geometry is the same as the previous case. Figure 13 presents the nondimensional frequencies $\lambda = \omega a\sqrt{v_{12}/E_2}$ for the pretwisted moderately deep shell with $\phi = 30^\circ$. The lower frequencies are not greatly influenced for all orientations considered. All frequencies near $\theta = 20^\circ$ are higher than those for any other orientation. For a shallow conical shell of $\phi = 10^\circ$, all frequencies are lower than those of $\phi = 30^\circ$ as shown in Figure 14. The fundamental frequencies are almost constant for all fiber orientations. The second frequencies decrease slightly with increase in fiber orientation.

5. CONCLUSIONS

The vibration characteristics of twisted cantilevered structures have been investigated using the finite element method with assumed strain based on Hellinger–Reissner principle. The present method used a degenerated solid shell element for the application of twisted conical shell. With a small number of elements, the present method has excellent convergence. Vibration frequencies and mode shapes for various twisted cylindrical and conical shells have been presented. The fundamental mode was affected substantially by shallowness ratio. For a slightly curved shell with large shallowness, there is no significant change in the fundamental frequency and mode shapes. As the twisting angle increases, frequencies of twisting modes increase significantly but frequencies of higher bending modes decrease.

ACKNOWLEDGMENTS

This work was supported through funding from the Korea Ministry of Science and Technology. The authors acknowledge the support (Subject No. 2000-N-NL-01-C-250) as the National Research Laboratory Program.

REFERENCES

1. A. W. Leissa 1973 *NASA SP*-288. Vibration of shells.
2. C. H. Chang 1981 *The Shock and Vibration Digest* **13**, 9–17. Vibration of conical shells.
3. R. K. Kapania 1989 *Transactions of the American Society of Mechanical Engineers Journal of Pressure Vessel Technology* **111**, 88–96. A review on the analysis of laminated shells.
4. S. Mirza 1991 *Transactions of the American Society of Mechanical Engineers Journal of Pressure Vessel Technology* **113**, 321–325. Recent research in vibration of layered shells.
5. C. Shu 1996 *International Journal of Mechanical and Sciences* **38**, 935–949. An efficient approach for free vibration analysis of conical shells
6. R. S. Srinivasan and P. A. Krishnan 1987 *Journal of Sound and Vibration* **117**, 153–160. Free vibration of conical shell panels.
7. C. W. Lim and K. M. Liew 1995 *Engineering Structures* **17**, 63–70. Vibratory behaviour of shallow conical shells by a global Ritz formulation.
8. C. W. Lim and K. M. Liew 1998 *International Journal of Solids Structures* **35**, 1695–1707. Vibration of cantilevered laminated composite shallow conical shells.
9. M. Petyt 1971 *Journal of Sound and Vibration* **15**, 381–395. Vibration of curved plates.
10. E. F. Crawley 1979 *Journal of composite Materials* **3**, 195–205. The natural modes of Graphite/Epoxy cantilevered plates and shells.
11. A. Nosier and J. N. Reddy 1992 *Journal of Sound and Vibration* **157**, 139–159. Vibration and stability analysis of cross-ply laminated circular cylindrical shells.
12. A. Selmane and A. A. Lakis 1997 C*omputers and Structures* **62**, 1–12. Dynamic analysis of anisotropic open cylindrical shells.

13. O. ATTIA and A. EL-ZAFRANY 1999 *International Journal of Mechanical and Sciences* **41**, 461–486. A higher-order shear element for nonlinear vibration analysis of composite layered plates and shells.
14. H. PARISH 1979 *Computational Methods in Applied Mechanics and Engineering* **20**, 323–350. A critical survey of the nine-node degenerated shell element with special emphasis on thin shell application and reduced integration.
15. S. W. LEE and T. H. H. PIAN 1978 *American Institute of Aeronautical and Astronautics Journal* **16**, 29–34. Improvement of plate and shell finite element by mixed formulations.
16. C. H. YEOM and S. W. LEE 1989 *International Journal of Numerical Methods in Engineering* **28**, 1749–1768. An assumed strain finite element model for large deflection composite shells.
17. C. H. YEOM and S. W. LEE 1991 *International Journal of Numerical Methods in Engineering* **31**, 287–305. On strain assumption in a finite element model for plates and shells.
18. S. AHMAD and B. M. IRONS 1970 *International Journal of Numerical Methods in Engineering* **21**, 419–451. Analysis of thick and thin shell structures by cured elements.